ELSEVIER

Journal of Alloys and Compounds 323–324 (2001) 509–512

Journal of ALLOYS AND COMPOUNDS

www.elsevier.com/locate/jallcom

Magnetic ordering and crystalline electric field splitting in $Nd_3Pd_{20}Si_6$

T. Herrmannsdörfer[a,*], A. Dönni[b], P. Fischer[a], L. Keller[a], E. Clementyev[a], A. Furrer[a], S. Mango[c], B. van den Brandt[c], H. Kitazawa[d]

[a]*Laboratory for Neutron Scattering, ETH Zürich and Paul Scherrer Institute, CH-5232 Villigen PSI, Switzerland*
[b]*Department of Physics, Niigata University, Niigata 950-2181, Japan*
[c]*Low Temperature Facilities, Paul Scherrer Institute, CH-5232 Villigen PSI, Switzerland*
[d]*National Research Institute for Metals (NRIM), Tsukuba 305-0047, Ibaraki, Japan*

Abstract

At the temperatures $T_{N1} \approx 2.4$ K and $T_{N2} \approx 0.7$ K, the cubic intermetallic compound $Nd_3Pd_{20}Si_6$ undergoes second order magnetic phase transitions. Here we report on the magnetic structures obtained from low-temperature neutron diffraction data by using a He dilution refrigerator, and on the crystalline electric field splitting of the Nd^{3+} ground state multiplet $^4I_{9/2}$ obtained from inelastic neutron scattering data.

Keywords: Intermetallics; Magnetically ordered materials; Crystal and ligand fields; Phase transitions; Neutron scattering

1. Introduction

$Nd_3Pd_{20}Si_6$ belongs to a class of intermetallic compounds with general formula $R_3Pd_{20}X_6$ (3-20-6) that form with all rare earths for X=Si and with only the light rare earths for X=Ge. The compounds crystallise in a cubic structure with space group $Fm\bar{3}m$, No. 225, $Z=4$, and the rare-earth ions occupy the two crystallographic sites *8c* and *4a*. Both Nd sites have cubic point symmetry, but different coordination polyhedra. It has been found that the compounds $Nd_3Pd_{20}Ge_6$, $Tb_3Pd_{20}Si_6$, and $Dy_3Pd_{20}Si_6$ undergo successive magnetic phase transitions [1–4]: below the higher ordering temperature T_{N1}, the *8c* sites are ordered with a propagation vector $\mathbf{k_1}=[1,1,1]$ in an antiferromagnetic sequence of ferromagnetic (111)-planes along the [111]-direction, whereas the *4a* sites remain in disorder down to the lower ordering temperature T_{N2}, where they also enter an antiferromagnetically ordered state of AF-I type ($\mathbf{k_2}=[0,0,1]$). Recently, a third magnetic phase transition in $Nd_3Pd_{20}Ge_6$ between T_{N1} and T_{N2} has been identified to originate from atomic disorder, resulting in a weak incommensurate perturbation with $\mathbf{k_{1i}}=[\tau,\tau,\tau]$, $\tau=0.79$ [2,5]. The crystalline electric field (CEF) level scheme of $Nd_3Pd_{20}Ge_6$ was reported to be $\Gamma_8^{(1)} \rightarrow \Gamma_6$ (1.85 meV)$\rightarrow\Gamma_8^{(2)}$ (4.55 meV) [1], and although it is expected that the different crystalline surroundings of the Nd sites *8c* and *4a* should reflect into two sets of CEF transitions, only one CEF level scheme was observed, similarly to the case of $Pr_3Pd_{20}Ge_6$ [6]. We have performed both elastic and inelastic neutron scattering experiments on a polycrystalline sample of $Nd_3Pd_{20}Si_6$ and compare the results with those of the $Nd_3Pd_{20}Ge_6$ studies.

2. Experimental procedure

Polycrystalline $Nd_3Pd_{20}Si_6$ was prepared by arc-melting stoichiometric amounts of the starting materials in an argon gas atmosphere and subsequent annealing in an evacuated quartz tube. The sample was filled under He atmosphere into V and Al cylinders of 8-mm diameter and ~5-cm height for the elastic and inelastic measurements, respectively.

Neutron diffraction data were collected at the instrument DMC, situated at a supermirror neutron guide at the Swiss spallation neutron source SINQ, PSI Villigen. A wavelength of $\lambda=2.561$ Å was selected from the 002 reflection of a vertically focusing graphite monochromator in combination with a pyrolytic graphite filter reducing higher-order contamination. In order to access several temperatures in the range between 125 mK and 3.5 K, we used a $^3He/^4He$ dilution cryostat designed by the low temperature facilities

*Corresponding author. Tel.: +41-56-310-4374; fax: +41-56-310-2939.

E-mail address: thilo.herrmannsdoerfer@psi.ch (T. Herrmannsdörfer).

0925-8388/01/$ – see front matter
PII: S0925-8388(01)01024-6

group at PSI. The inelastic measurements were performed at the SINQ triple-axis spectrometer DrüchaL. The final energy was fixed at 4.7 meV and a cold Be-filter was placed between the sample and the analyser in order to remove higher order neutrons. Energy scans were performed at constant moduli of the scattering vector **Q** of 1.60 and 2.40 $Å^{-1}$. The energy resolution at the elastic peak was 0.17 meV (FWHM). A standard ILL type orange cryostat was used to record spectra in the paramagnetic state at temperatures between 5 and 50 K.

3. Results

3.1. The magnetic structure of $Nd_3Pd_{20}Si_6$

Fig. 1 shows a refinement of the magnetic neutron powder diffraction data of $Nd_3Pd_{20}Si_6$, obtained by subtracting the paramagnetic intensities measured at $T=3.5$ K from those taken in the fully ordered state at $T=0.125$ K. Similar to other $R_3Pd_{20}Si_6$ compounds as mentioned above, our neutron data confirm for $Nd_3Pd_{20}Si_6$ two phase transitions that are associated with the propagation vectors $\mathbf{k_1}=[1,1,1]$ and $\mathbf{k_2}=[0,0,1]$, respectively. Due to different reflection conditions, they can be associated with a successive magnetic ordering at the *8c* (simple cubic sublattice) and the *4a* (F-centred sublattice) sites, respectively.

As can be seen from Fig. 2, the *8c* magnetic moments are fully saturated at $T=0.125$ K and the *4a* magnetic moments are close to saturation. The magnitudes of the ordered magnetic Nd moments at $T=0.125$ K are $\mu_{8c}=2.52(3)\ \mu_B$ and $\mu_{4a}=2.26(6)\ \mu_B$. Due to CEF effects, both values are reduced compared to the free ion value of 3.27 μ_B. Below 0.2 K, a small upturn in the temperature dependence of the magnetic moments may presumably be regarded as a contribution from ordering of the nuclear Nd spins, which was also observed for $Nd_3Pd_{20}Ge_6$ [2]. The construction principle of the dilution cryostat did not allow for controlled operation between 1.2 and 3.5 K, therefore the evolution of the *8c* sublattice ordering will be subject to additional measurements with a conventional cryostat.

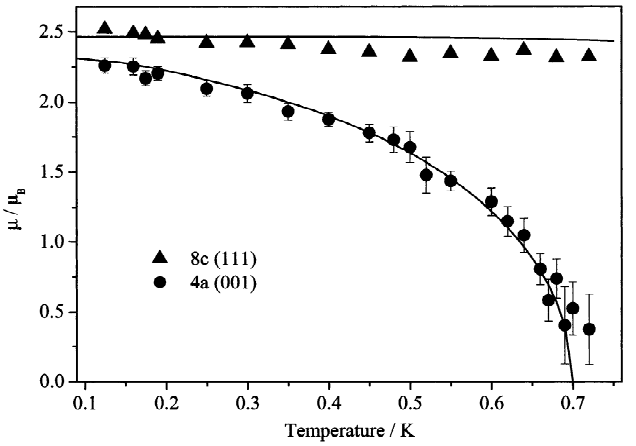

Fig. 2. The temperature dependence of the magnetic Nd moments at the *8c* and the *4a* sites, obtained from the integrated neutron intensities of the $Nd_3Pd_{20}Si_6$ magnetic (111) and (001) Bragg reflections, respectively. The error bars of the (111) data correspond to the size of the data points and are therefore omitted. The solid lines represent calculated values based on the crystal-field parameters given in the text.

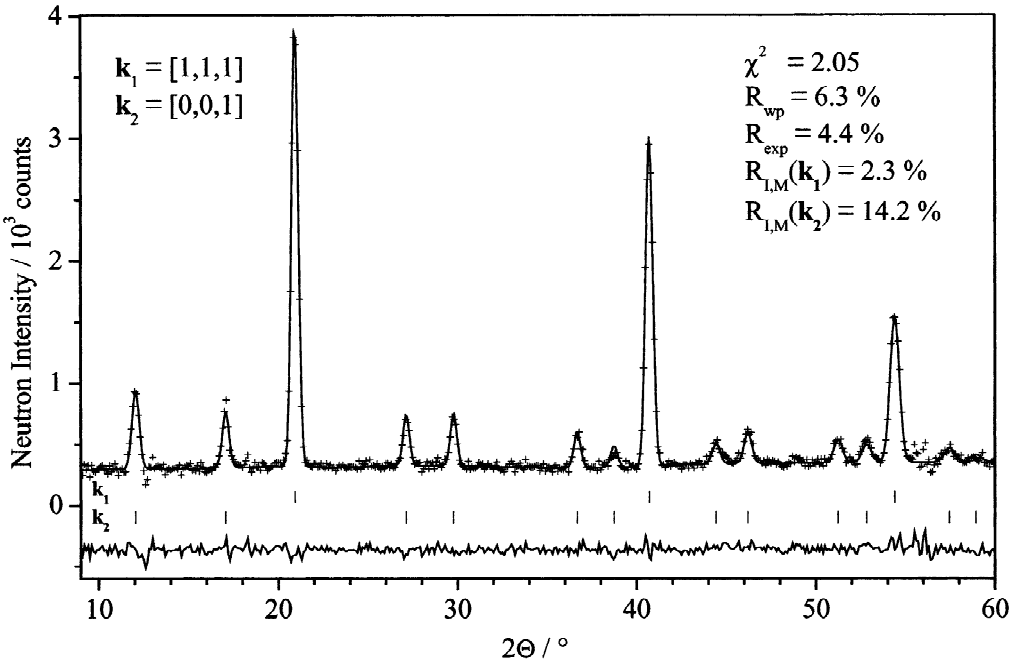

Fig. 1. Observed, calculated and difference magnetic neutron powder diffraction pattern of $Nd_3Pd_{20}Si_6$ ($I_{0.13\ K}-I_{3.5\ K}+400$). R_{wp}, R_{exp}, $R_{I,M}$: agreement factors describing weighted-profile, expected counting statistics and integrated magnetic neutron intensities, respectively.

The lower ordering temperature $T_{N2} \approx 0.7$ K is in good agreement with Ref. [7].

Since the configurational symmetry of the *8c* sites in the ordered state is cubic, the direction of the magnetic moments remains undetermined in a zero field powder diffraction experiment. For the *4a* sites, the angle α_2 between $\mathbf{k}_2$ and the magnetic moments can be extracted and was refined to 68(5)°. This is to be compared to $Nd_3Pd_{20}Ge_6$, $Tb_3Pd_{20}Si_6$ and $Dy_3Pd_{20}Si_6$, where α_2 was reported to be 90°, 0°, and 54.7°, respectively [2–4]. The corresponding magnetic structure of $Nd_3Pd_{20}Ge_6$ is illustrated in Fig. 3.

3.2. The crystalline electric field excitations of $Nd_3Pd_{20}Si_6$

The degeneracy of the $^4I_{9/2}$ ground state multiplet of Nd^{3+} is partly removed by the influence of the electric charge distribution of the surrounding ions. For both Nd sites, the Hamiltonian for cubic symmetry

$$H_{CEF} = B_4(O_4^0 + 5O_4^4) + B_6(O_6^0 - 21O_6^4) \quad (1)$$

decomposes the Nd^{3+} J-multiplet into a doublet Γ_6 and two quartets $\Gamma_8^{(1)}$ and $\Gamma_8^{(2)}$. B_4 and B_6 are the adjustable crystal-field parameters and the O_n^m are the Stevens Operator equivalents [8].

Fig. 4 shows the energy spectrum of $Nd_3Pd_{20}Si_6$, collected in the paramagnetic state at $T = 25$ K. Four well defined lines, labelled A–D, can be identified in the spectrum. The lines were confirmed to be of magnetic origin by a measurement at a higher Q value. One can immediately conclude that the energy spectra cannot be explained within a single cubic CEF level scheme. When the temperature is increased, the intensities of the A, B and D lines decrease, whereas C increases intensity with temperature. A, B and D can therefore be identified as excitations out of the ground state, whereas C is originating from an excited state. The energies of A, B and C form a triple such that $E_A + E_C = E_B$. Therefore, it is concluded that these lines can be attributed to the CEF excitations of either the *8c* or the *4a* Nd sites. From the remaining line D, the CEF level scheme for the other Nd site can not at present be unambiguously determined. Starting from the crystal-field parameters given in Ref. [1], we found that the observed intensities of A, B and C can well be explained assuming the following CEF level scheme: $\Gamma_8^{(1)} \rightarrow \Gamma_6$ (1.38 meV) $\rightarrow \Gamma_8^{(2)}$ (5.01 meV) (Fig. 5). The corresponding crystal-field parameters are $B_4 = 7.16 \times 10^{-4}$ meV and $B_6 = 1.59 \times 10^{-5}$ meV, leading to a very good agreement between the observed and the calculated intensities. The expected value of the magnetic saturation moment along the [0,0,1] direction, calculated from these crystal-field parameters, is 2.47 μ_B. This is in excellent agreement with the observed value from the diffraction data for the *8c* sites, $\mu_{8c} = 2.52(3)$ μ_B, if one keeps in mind the small nuclear Nd spin contribution (Fig. 2). Therefore we may favour the assumption that the proposed CEF level scheme actually belongs to the *8c* sites.

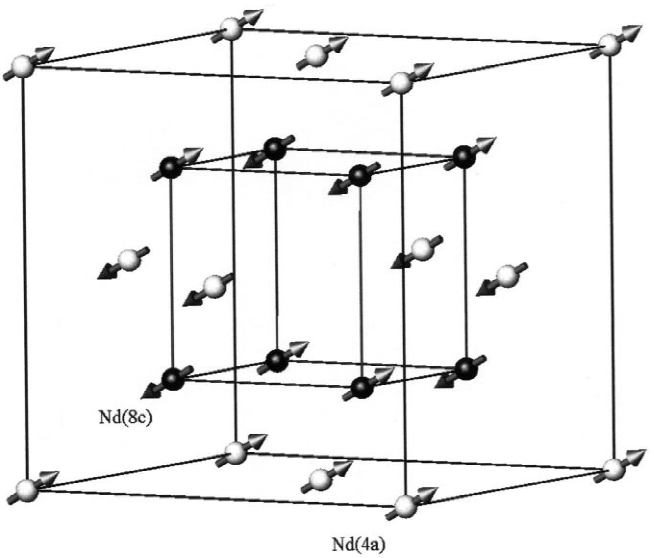

Fig. 3. Antiferromagnetic arrangement of the magnetic Nd moments of $Nd_3Pd_{20}Si_6$ at temperatures below T_{N2}.

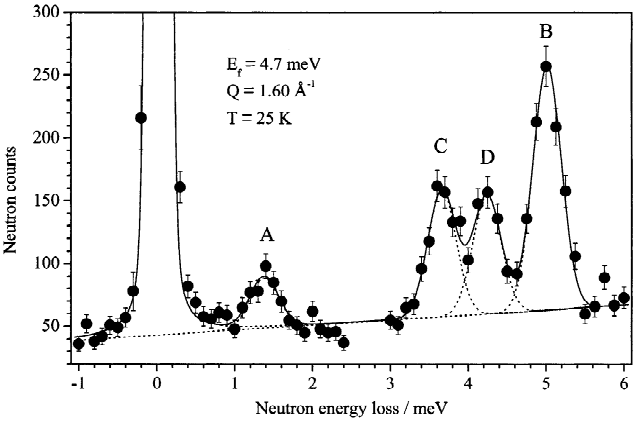

Fig. 4. Neutron energy spectrum of $Nd_3Pd_{20}Si_6$ at $T = 25$ K and $Q = 1.60$ Å^{-1}. The solid line represents a least-squares fit of Gaussian peaks (dotted lines) to the observed data. The region between 2.5 and 3.0 meV contains no excitations and was omitted for the measurement at 25 K.

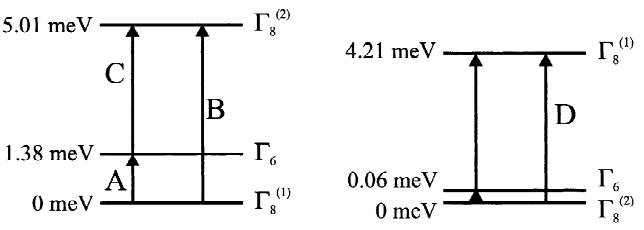

Fig. 5. The proposed CEF level schemes for the two Nd sites of $Nd_3Pd_{20}Si_6$. The labels of the transitions correspond to the labels given in Fig. 4.

The *8c* sites have 12 Pd and 6 Si nearest neighbours, and the *4a* sites are surrounded by 16 Pd atoms (see, for example, Fig. 3 in Ref. [1]). One may take the CEF parameters given above and extrapolate them to the other Nd site, using the two sets of the Nd nearest neighbours coordinates as an input for the calculation of the geometrical part of the CEF potential. From this, we obtained starting values for the parameters B_4 and B_6, leading to the CEF level scheme $\Gamma_8^{(2)} \rightarrow \Gamma_6$ (0.06 meV)$\rightarrow \Gamma_8^{(1)}$ (4.21 meV) with $B_4 = -1.06 \times 10^{-3}$ meV and $B_6 = -5.25 \times 10^{-6}$ meV. Since these energies are very close to a crossover from the $\Gamma_8^{(2)}$ to the Γ_6 ground state and the experimental resolution did not allow to resolve the lower transition, a measurement with better resolution will be needed in order to check the correctness of this model. A least-squares fit of the two CEF level schemes with a ratio of 2:1 for the number of Nd atoms yielded a very good agreement between the observed and the calculated intensities ($\chi^2 = 1.6$), supporting the assumption that the latter scheme belongs to the *4a* sites.

We have calculated the temperature dependence of the magnetic Nd moments on the basis of our preliminary CEF model for the *4a* sites. The crystal field produces a rather high anisotropy, resulting in a strong angular dependence of the ordered magnetic moment. For the calculations, the moment direction was constrained to have an angle α_2 of 68°, corresponding to the experimental value of the diffraction data. As can be seen from Fig. 2, this leads to an exceptionally good agreement between the observed and the calculated data, giving a nice example of the complementarity between the elastic and the inelastic measurements and further supporting our proposed CEF parameters.

4. Conclusions

We have performed elastic and inelastic neutron scattering experiments on $Nd_3Pd_{20}Si_6$. The two Nd sites *8c* and *4a* undergo a successive antiferromagnetic ordering with $\mathbf{k_1} = [1,1,1]$ and $\mathbf{k_2} = [0,0,1]$, respectively. The inelastic measurements show a clear signature of two different crystalline electric field level schemes for the two Nd sites. The CEF levels for one of the Nd sites was determined to be $\Gamma_8^{(1)} \rightarrow \Gamma_6$ (1.38 meV)$\rightarrow \Gamma_8^{(2)}$ (5.01 meV) and is likely to be attributed to the *8c* sites. For the *4a* sites, we propose the model $\Gamma_8^{(2)} \rightarrow \Gamma_6$ (0.06 meV)$\rightarrow \Gamma_8^{(1)}$ (4.21 meV). A comparative crystal-field study of other members of the $R_3Pd_{20}Si_6$ series is currently in progress.

Acknowledgements

Partial support from the Swiss National Science Foundation is gratefully acknowledged.

References

[1] A. Dönni, L. Keller, P. Fischer, Y. Aoki, H. Sato, F. Fauth, M. Zolliker, T. Komatsubara, Y. Endoh, J. Phys. Condens. Matter. 10 (1998) 7219.

[2] A. Dönni, F. Fauth, P. Fischer, T. Herrmannsdörfer, L. Keller, T. Komatsubara, J. Alloys Comp. 306 (2000) 40.

[3] T. Herrmannsdörfer, A. Dönni, P. Fischer, L. Keller, G. Böttger, M. Gutmann, H. Kitazawa, J. Tang, J. Phys. Condens. Matter. 11 (1999) 2929.

[4] T. Herrmannsdörfer, A. Dönni, P. Fischer, L. Keller, H. Kitzawa, Physica B 281–282 (2000) 167.

[5] J. Kitagawa, N. Takeda, F. Sakai, M. Ishikawa, J. Phys. Soc. Jpn. 68 (1999) 3413.

[6] L. Keller, A. Dönni, M. Zolliker, T. Komatsubara, Physica B 259–261 (1999) 336.

[7] J. Kitagawa, N. Takeda, M. Ishikawa, J. Alloys Comp. 256 (1997) 48.

[8] K.W.H. Stevens, Proc. Phys. Soc. A 65 (1952) 209.